coatings

MDPI

Article

Significance of Arrhenius Activation Energy and Binary Chemical Reaction in Mixed Convection Flow of Nanofluid Due to a Rotating Disk

Metib Alghamdi

Department of Mathematics, College of Science, King Khalid University, Abha 61413, Saudi Arabia; malgamdy@kku.edu.sa

Received: 10 December 2019; Accepted: 16 January 2020; Published: 20 January 2020

Abstract: This article addresses mixed convective 3D nanoliquid flow by a rotating disk with activation energy and magnetic field. Flow was created by a rotating disk. Velocity, concentration and temperature slips at the surface of a rotating disk were considered. Impacts of Brownian diffusion and thermophoretic were additionally accounted for. The non-linear frameworks are simplified by suitable variables. The shooting method is utilized to develop the numerical solution of resulting problem. Plots were prepared just to explore that how concentration and temperature are impacted by different pertinent flow parameters. Sherwood and Nusselt numbers were additionally plotted and explored. Furthermore, the concentration and temperature were enhanced for larger values of Hartman number. However, the heat transfer rate (Nusselt number) diminishes when the thermophoresis parameter enlarges.

Keywords: rotating disk; mixed convective flow; MHD; binary chemical reaction; nanoparticles; arrhenius activation energy

1. Introduction

A nanoparticle of size under 100 nm deferred into a standard fluid is then named a nanofluid. The essentialness of a nanofluid is expected from its distinctive thermophysical qualities. Nanofluids show enormous capacity to lead power and heat, so they have a critical impact in industry. Nanoliquids have attracted extraordinary enthusiasm for their wide applications; for example, electronic chip cooling, hybrid powered machines, progressed atomic frameworks, solar liquid heating, microchips, excessively proficient magnets and optoelectronics. Thus, Choi [1] exhibited the term nanoparticle inundated into a standard fluid. Buongiorno [2] presented a mathematical model for heat transport in nanoliquid by considering the impacts of Brownian diffusion and thermophoretic dispersion. Further examinations on nanofluids can be seen through the attempts [3–28].

The flow due to a rotating disk plays vital roles in numerous mechanical processes, encompassing psychologist fits, rotors and flywheels. Recently rotating disks became very significant in thermal power creating frameworks, electric-control generation, stopping mechanisms, rotating sawing machines, etc. Fluid flow by a rotating disk is initiated by the Von Karman effect [29]. Turkyilmazoglu and Senel [30] explored the impacts of mass and heat transport because of the porous disk subject to rotating frame. Entropy generation in MHD flow by the rotation of porous disk subject to slip and variable properties is examined by Rashidi et al. [31]. Nanofluid flow because of revolution of disk is discussed by Turkyilmazoglu [32]. Hatami et al. [33] investigated the impacts of contracting rotating disk on nanofluids. They utilized least square technique for solution development. Mustafa et al. [34] analyzed three dimensional nanofluid flow over a stationary disk. Sheikholeslami et al. [35] constructed numerical solutions of nanofluid by a rotating surface. Micropolar liquid flow by a turning disk

is explored by Doh and Muthtamilselvan [36]. Aziz et al. [37] provided a numerical report to nanofluid flow by rotation of disk subject to slip impacts and thermal absorption/generation. Third-grade nanofluid flow over a stretchable rotating surface with heat generation is examined by Hayat et al. [38]. Radiative flow in the presence of nanoparticles and gyrotactic microorganism by the variable-in-thickness surface of a pivoting disk is explained by Qayyum et al. [39]. Hayat et al. [40] provided a numerical solution for radiative flow of carbon nanotubes by the revolution of disk subject to partial slip.

The aim of the present paper is to generalize the analysis of study [11] into four directions. Firstly, to examine magnetohydrodynamic flow of viscous nanofluid due to the rotation of disk. Attention is mainly given to Brownian diffusion and thermophoresis. Secondly, to utilize thermal, concentration and velocity slips at the surface of rotating disk. Thirdly, to consider the effect of mixed convection. Fourth, to analyze the Arrhenius activation energy and binary chemical reaction. The resulting scientific framework is solved numerically via the shooting method. Concentration, temperature and Sherwood and Nusselt numbers are also explored via graphs.

2. Problem Description

Let us examine a mixed convective 3D nanoliquid flow by a pivoting disk with slip features. Arrhenius activation energy, magnetic field and binary chemical reaction are also accounted for. A disk at $z = 0$ rotates with constant angular velocity Ω (see Figure 1). Brownian dispersion and thermophoretic impacts are additionally present. The velocities are (u, v, w) in the headings of expanding (r, φ, z) respectively. The associated boundary-layer equations are [11,37]:

$$\frac{\partial u}{\partial r} + \frac{u}{r} + \frac{\partial w}{\partial z} = 0, \tag{1}$$

$$u\frac{\partial u}{\partial r} - \frac{v^2}{r} + w\frac{\partial u}{\partial z} = \nu\left(\frac{\partial^2 u}{\partial z^2} + \frac{\partial^2 u}{\partial r^2} + \frac{1}{r}\frac{\partial u}{\partial r} - \frac{u}{r^2}\right) - \frac{\sigma B_0^2}{\rho_f}u + g^*(\beta_T\,(T - T_\infty) + \beta_C\,(C - C_\infty)), \tag{2}$$

$$u\frac{\partial v}{\partial r} + \frac{uv}{r} + w\frac{\partial v}{\partial z} = \nu\left(\frac{\partial^2 v}{\partial z^2} + \frac{\partial^2 v}{\partial r^2} + \frac{1}{r}\frac{\partial v}{\partial r} - \frac{v}{r^2}\right) - \frac{\sigma B_0^2}{\rho_f}v, \tag{3}$$

$$u\frac{\partial w}{\partial r} + w\frac{\partial w}{\partial z} = \nu\left(\frac{\partial^2 w}{\partial r^2} + \frac{\partial^2 w}{\partial z^2} + \frac{1}{r}\frac{\partial w}{\partial r}\right), \tag{4}$$

$$\begin{aligned} u\frac{\partial T}{\partial r} + w\frac{\partial T}{\partial z} &= \alpha_m\left(\frac{\partial^2 T}{\partial r^2} + \frac{\partial^2 T}{\partial z^2} + \frac{1}{r}\frac{\partial T}{\partial r}\right) \\ &+ \frac{(\rho c)_p}{(\rho c)_f}\left(D_B\left(\frac{\partial T}{\partial r}\frac{\partial C}{\partial r} + \frac{\partial T}{\partial z}\frac{\partial C}{\partial z}\right) + \frac{D_T}{T_\infty}\left(\left(\frac{\partial T}{\partial z}\right)^2 + \left(\frac{\partial T}{\partial r}\right)^2\right)\right), \end{aligned} \tag{5}$$

$$\begin{aligned} u\frac{\partial C}{\partial r} + w\frac{\partial C}{\partial z} &= D_B\left(\frac{\partial^2 C}{\partial r^2} + \frac{\partial^2 C}{\partial z^2} + \frac{1}{r}\frac{\partial C}{\partial r}\right) \\ &+ \frac{D_T}{T_\infty}\left(\frac{\partial^2 T}{\partial r^2} + \frac{\partial^2 T}{\partial z^2} + \frac{1}{r}\frac{\partial T}{\partial r}\right) - k_r^2\,(C - C_\infty)\left(\frac{T}{T_\infty}\right)^n \exp\left(-\frac{E_a}{\kappa T}\right), \end{aligned} \tag{6}$$

$$u = L_1\frac{\partial u}{\partial z},\ v = r\Omega + L_1\frac{\partial v}{\partial z},\ w = 0,\ T = T_w + L_2\frac{\partial T}{\partial z},\ C = C_w + L_3\frac{\partial C}{\partial z} \text{ at } z = 0, \tag{7}$$

$$u \to 0, \quad v \to 0, \quad T \to T_\infty, \quad C \to C_\infty \quad \text{as } z \to \infty. \tag{8}$$

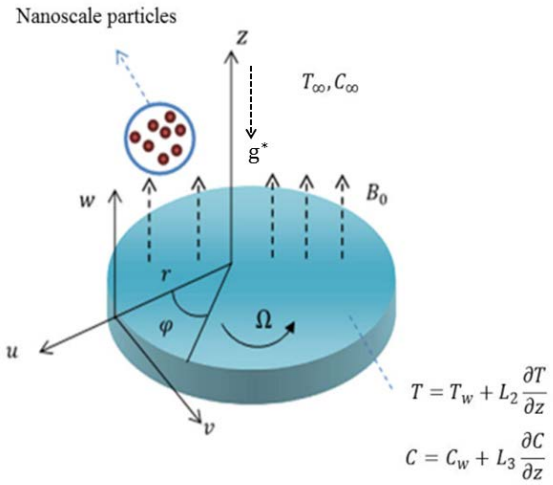

Figure 1. Schematic diagram of the problem.

Here u, v and w stand for velocity components in directions of r, φ and z; ρ_f, μ and $\nu = \mu/\rho_f$ are for fluid density, dynamic and kinematic viscosities, respectively. L_1 stands for velocity slip factor; C_∞ for ambient concentration; g^* for acceleration due to gravity; T_∞ for ambient temperature; β_T for thermal expansion factor; $(\rho c)_p$ for effective heat capacity of nanoparticles; σ for electrical conductivity; E_a for activation energy; L_3 for concentration slip factor; $(\rho c)_f$ for heat capacity of liquid; β_C for concentration expansion factor, C for concentration; L_2 for thermal slip factor; n for fitted rate constant; D_T for thermophoretic factor, $\alpha_m = k/(\rho c)_f$ and k for thermal diffusivity and thermal conductivity, respectively; k_r for reaction rate; T for fluid temperature; D_B for Brownian factor; and κ for Boltzmann constant. Selecting [37]:

$$\left.\begin{array}{c} u = r\Omega f'(\zeta),\ w = -(2\Omega\nu)^{1/2} f(\zeta),\ \theta(\zeta) = \frac{T-T_\infty}{T_w-T_\infty}, \\ \phi(\zeta) = \frac{C-C_\infty}{C_w-C_\infty},\ \zeta = \left(\frac{2\Omega}{\nu}\right)^{1/2} z,\ v = r\Omega g(\zeta). \end{array}\right\} \tag{9}$$

Equation (1) is now verified while Equations (2)–(8) yield [11,37]:

$$2f''' + 2ff'' - f'^2 + g^2 - (Ha)^2 f' + \lambda_T(\theta + \lambda_C\phi) = 0, \tag{10}$$

$$2g'' + 2fg' - 2f'g - (Ha)^2 g = 0, \tag{11}$$

$$\frac{1}{\mathrm{Pr}}\theta'' + f\theta' + N_b\theta'\phi' + N_t\theta'^2 = 0, \tag{12}$$

$$\frac{1}{Sc}\phi'' + f\phi' + \frac{1}{Sc}\frac{N_t}{N_b}\theta'' - \sigma(1+\delta\theta)^n \phi \exp\left(-\frac{E}{1+\delta\theta}\right) = 0, \tag{13}$$

$$f(0) = 0,\ f'(0) = \alpha f''(0),\ g(0) = 1 + \alpha g'(0),\ \theta(0) = 1 + \beta\theta'(0),\ \phi(0) = 1 + \gamma\phi'(0), \tag{14}$$

$$f'(\infty) \to 0,\ g(\infty) \to 0,\ \theta(\infty) \to 0,\ \phi(\infty) \to 0. \tag{15}$$

Here λ_T stands for thermal buoyancy number, N_t for thermophoresis parameter, α for velocity slip parameter, Pr for Prandtl number, λ_C for concentration buoyancy number, Sc for Schmidt parameter, Ha for Hartman number, β for thermal slip parameter, σ for chemical reaction number, N_b for Brownian parameter, δ for temperature difference parameter, γ for concentration slip parameter and E for non-dimensional activation energy. These parameters are defined by

$$\left.\begin{array}{c}(Ha)^2=\frac{\sigma B_0^2}{\Omega\rho_f},\ \mathrm{Pr}=\frac{\nu}{\alpha_m},\ \alpha=L_1\sqrt{\frac{2\Omega}{\nu}},\ \gamma=L_3\sqrt{\frac{2\Omega}{\nu}},\\ N_t=\frac{(\rho c)_p D_T(T_w-T_\infty)}{(\rho c)_f\nu T_\infty},\ Sc=\frac{\nu}{D_B},\ N_b=\frac{(\rho c)_p D_B(C_w-C_\infty)}{(\rho c)_f\nu},\ \lambda_T=\frac{g^*\beta_T\beta_T(T_w-T_\infty)}{\Omega},\\ \lambda_C=\frac{\beta_C(C_w-C_\infty)}{\beta_T(T_w-T_\infty)},\ \beta=L_2\sqrt{\frac{2\Omega}{\nu}},\ \sigma=\frac{k_r^2}{\Omega},\ \delta=\frac{T_w-T_\infty}{T_\infty},\ E=\frac{E_a}{\kappa T_\infty}.\end{array}\right\} \quad (16)$$

The coefficients of skin friction and Sherwood and Nusselt numbers are

$$\mathrm{Re}_r^{1/2}C_f=f''(0),\ \mathrm{Re}_r^{1/2}C_g=g'(0),\ \mathrm{Re}_r^{-1/2}Sh=-\phi'(0),\ \mathrm{Re}_r^{-1/2}Nu=-\theta'(0), \quad (17)$$

where $\mathrm{Re}_r=2(\Omega r)r/\nu$ depicts local rotational Reynolds number.

3. Solution Methodology

By employing suitable boundary conditions on the system of equations, a numerical solution was constructed considering NDSolve in Mathematica. The shooting method was employed via NDSolve. This method is very helpful in the situation of a smaller step-size featuring negligible error. As a consequence, both the z and r varied uniformly by a step-size of 0.01 [20].

4. Graphical Results and Discussion

This segment displays variations of various physical flow parameters, such as the thermophoresis parameter N_t, Hartman number Ha, thermal slip parameter β, chemical reaction parameter σ, Brownian motion parameter N_b, concentration slip parameter γ and activation energy E, on concentration $\phi(\zeta)$ and temperature $\theta(\zeta)$ distributions. Figure 2a displays the effect of Hartman number Ha on temperature $\theta(\zeta)$. Temperature $\theta(\zeta)$ is enhanced for higher estimations of Ha. The effect of thermal slip β on temperature $\theta(\zeta)$ is shown in Figure 2b. Greater β shows diminishing trend of $\theta(\zeta)$ and associated warmth layer. The impact of N_t on temperature $\theta(\zeta)$ is explored in Figure 2c. An increment in N_t leads to stronger temperature field $\theta(\zeta)$. Figure 2d depicts change in temperature $\theta(\zeta)$ for varying Brownian motion number N_b. Physically, the Brownian motion of nanoparticles is enhanced by increasing Brownian motion number N_b. Therefore dynamic vitality is altered into thermal vitality, which depicts an increment in temperature $\theta(\zeta)$ and the respective warmth layer. Figure 3a shows that how the Hartman number Ha influences concentration $\phi(\zeta)$. For a greater Hartman number Ha, both concentration $\phi(\zeta)$ and the concentration layer are upgraded. Figure 3b displays that concentration $\phi(\zeta)$ is weaker for a greater concentration slip. Figure 3c demonstrates how thermophoresis N_t influences concentration $\phi(\zeta)$. By improving the thermophoresis parameter N_t, the concentration $\phi(\zeta)$ and associated layer are upgraded. Figure 3d depicts effect of Brownian motion N_b on concentration $\phi(\zeta)$. It is noted that higher concentration $\phi(\zeta)$ is developed by utilizing greater Brownian parameter N_b. Figure 3e explains effect of non-dimensional activation energy E on concentration $\phi(\zeta)$. An increment in E rots change Arrhenius work $\left(\frac{T}{T_\infty}\right)^n \exp\left(-\frac{E_a}{\kappa T}\right)$, which inevitably builds up a generative synthetic reaction due to which concentration $\phi(\zeta)$ increases. Figure 3f introduces the fact that an increment in chemical response number σ causes a rot in concentration $\phi(\zeta)$. Figure 4a,b displays the effects of N_t and N_b on $\mathrm{Re}_r^{-1/2}Nu$. It is noted that $\mathrm{Re}_r^{-1/2}Nu$ decreases for greater N_t and N_b. Contributions of N_t and N_b on $\mathrm{Re}_r^{-1/2}Sh$ are explored in Figure 5a,b. Here $\mathrm{Re}_r^{-1/2}Sh$ is increasing the factor of N_b while it is decreasing the factor of N_t.

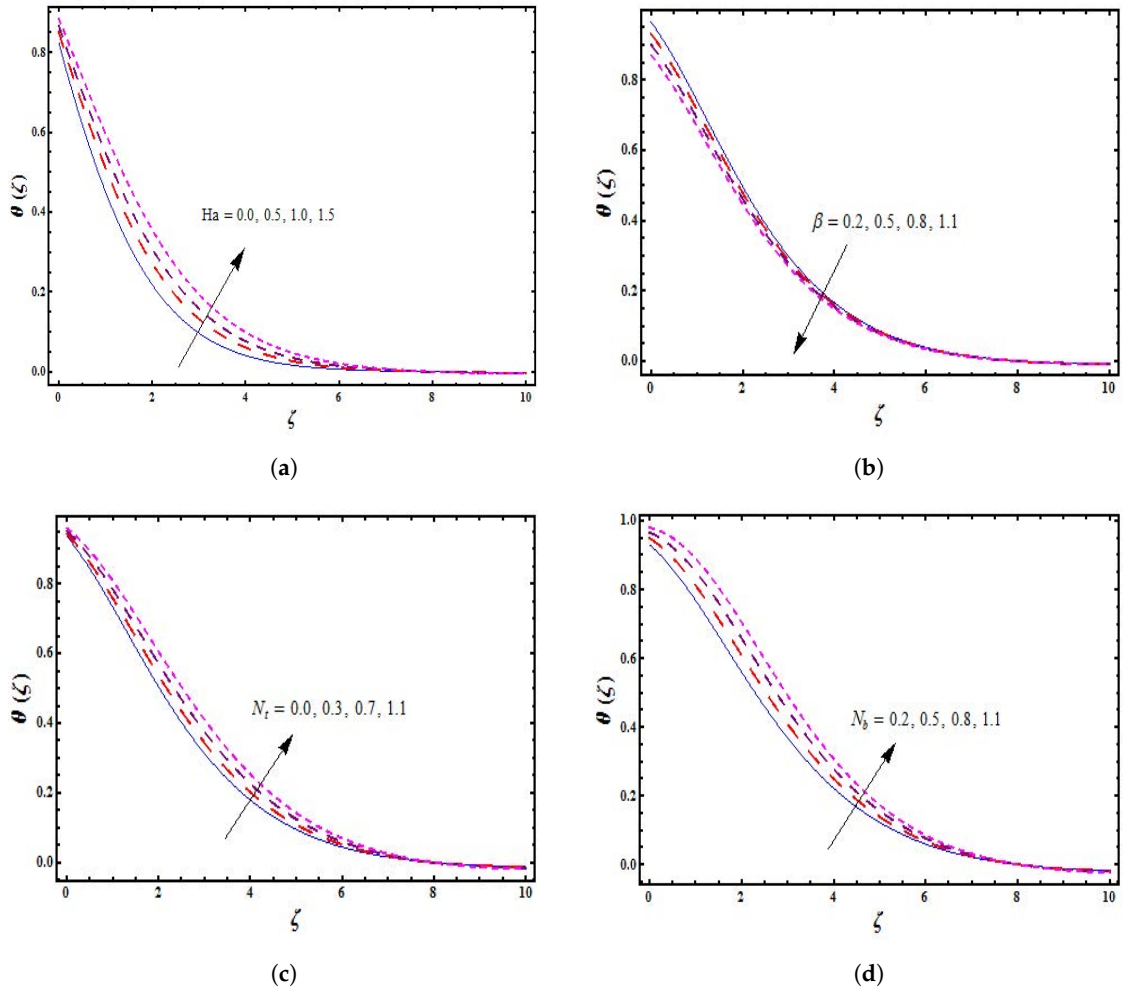

Figure 2. (**a**) Variations of temperature distribution $\theta(\zeta)$ for Hartman number Ha; (**b**) variations of temperature distribution $\theta(\zeta)$ for thermal slip parameter β; (**c**) variations of temperature distribution $\theta(\zeta)$ for thermophoresis parameter N_t; (**d**) variations of temperature distribution $\theta(\zeta)$ for Brownian motion parameter N_b.

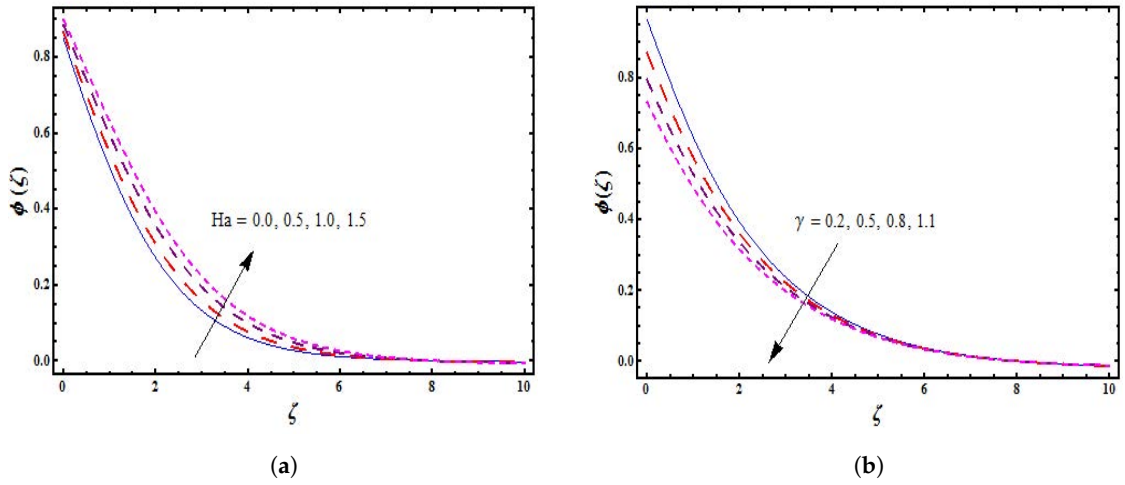

Figure 3. *Cont.*

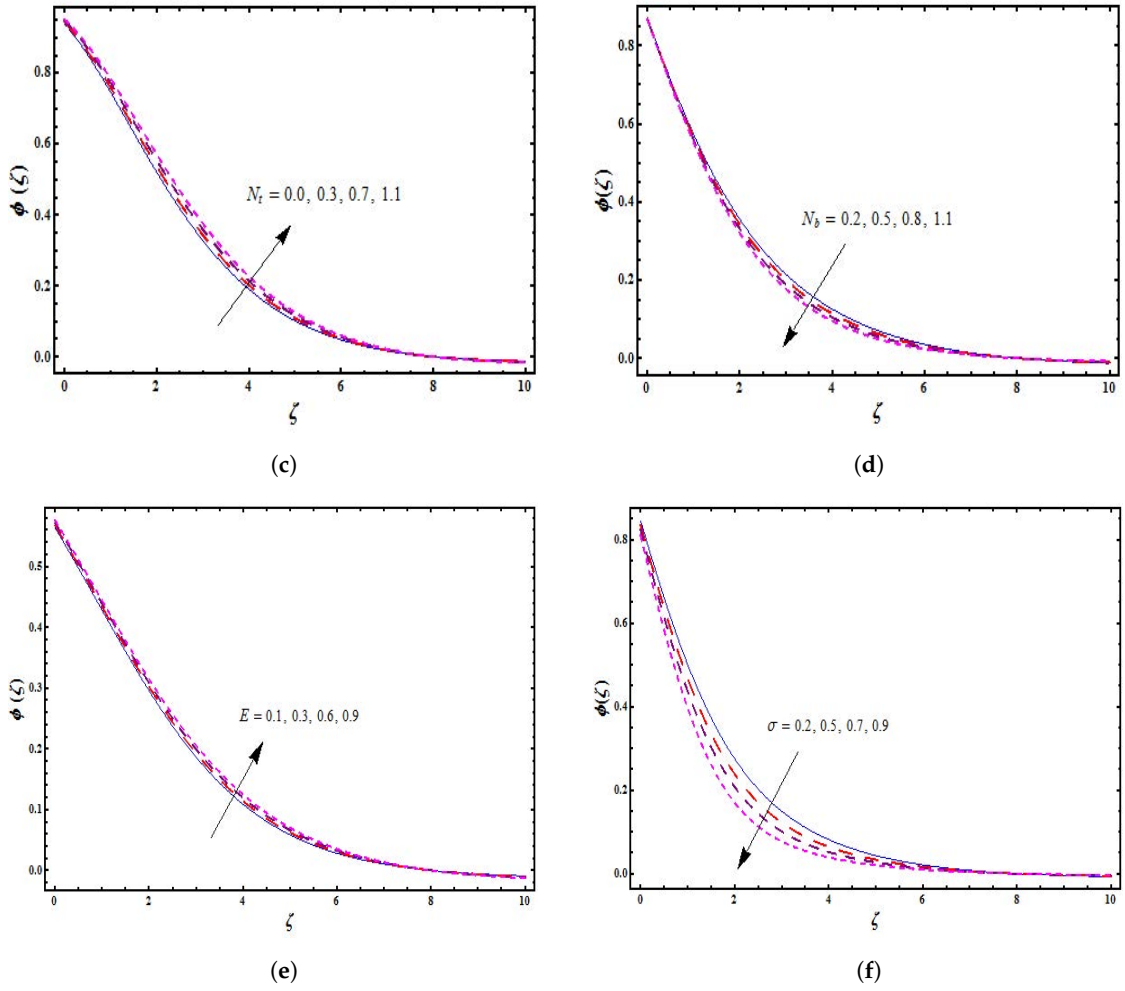

Figure 3. (**a**) Variations of concentration distribution $\phi(\zeta)$ for Hartman number Ha; (**b**) variations of concentration distribution $\phi(\zeta)$ for concentration slip parameter γ; (**c**) variations of concentration distribution $\phi(\zeta)$ for thermophoresis parameter N_t; (**d**) variations of concentration distribution $\phi(\zeta)$ for Brownian motion parameter N_b; (**e**) variations of concentration distribution $\phi(\zeta)$ for activation energy E; (**f**) variations of concentration distribution $\phi(\zeta)$ for chemical reaction parameter σ.

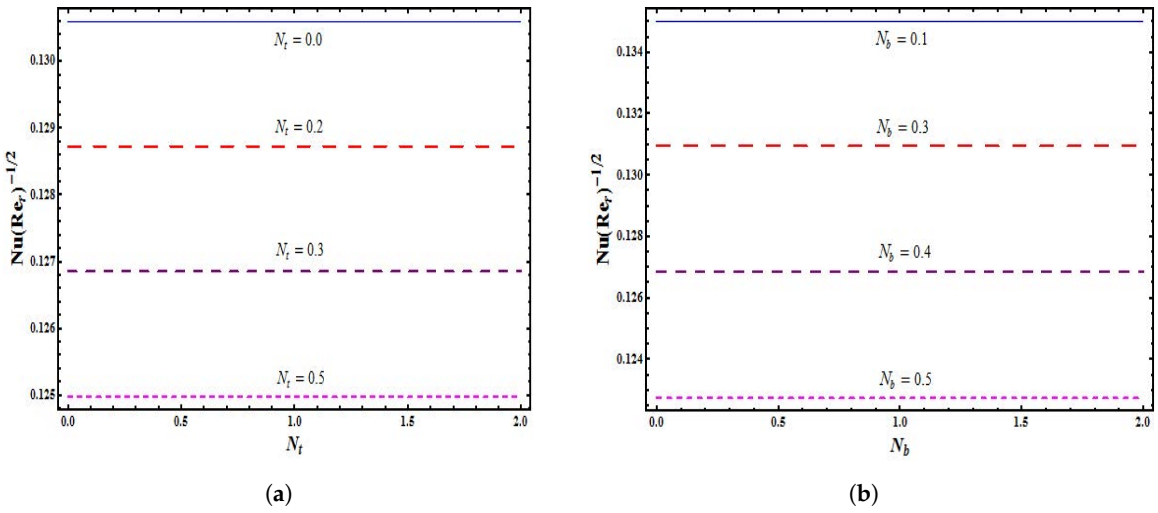

Figure 4. (**a**) Variations of Nusselt number $\mathrm{Re}_r^{-1/2}\,Nu$ for thermophoresis parameter N_t; (**b**) variations of Nusselt number $\mathrm{Re}_r^{-1/2}\,Nu$ for Brownian motion parameter N_b.

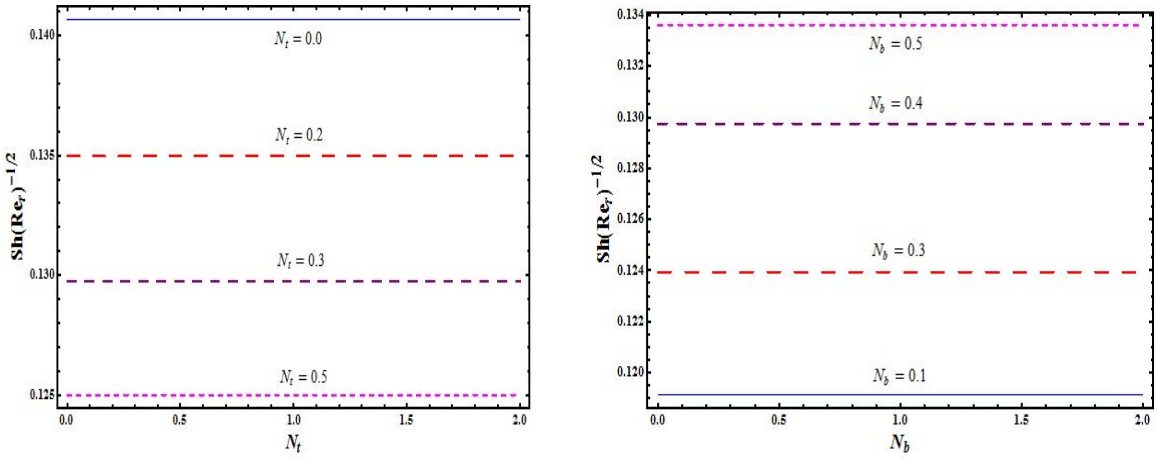

(**a**) (**b**)

Figure 5. (**a**) Variations of Sherwood number $\mathrm{Re}_r^{-1/2}\,Sh$ for thermophoresis parameter N_t; (**b**) variations of Sherwood number $\mathrm{Re}_r^{-1/2}\,Sh$ for Brownian motion parameter N_b.

5. Conclusions

Mixed convective 3D nanoliquid flow by a rotating disk subject to activation energy, magnetohydrodynamics and a binary chemical reaction was studied. Here, the flow field was considered to contain the chemically reacting species. Moreover, the mass transport mechanism was developed via modified Arrhenius function for the activation energy. Activation energy is the minimum quantity of energy needed by reactants to examine a chemical reaction. The source of the activation energy needed to initiate a chemical reaction is typically heat energy from the surroundings. Furthermore, the scientific system obtained was solved numerically via shooting method. A stronger temperature distribution was seen for N_b and N_t. Both the concentration and temperature display increasing behavior for greater Ha. Higher γ exhibits a decreasing trend for concentration field. Concentration $\phi(\zeta)$ depicts decreasing behavior for larger σ. Higher activation energy E shows stronger concentration $\phi(\zeta)$. Concentration $\phi(\zeta)$ displays reverse behavior for N_b and N_t.

Funding: This research was funded by the Deanship of Scientific Research, King Khalid University, Abha, Saudi Arabia under grant number (R.G.P.2./26/40).

Acknowledgments: The author extends his appreciation to the Deanship of Scientific Research at King Khalid University for funding this work through Research Groups Program under grant number (R.G.P.2./26/40).

Conflicts of Interest: The author declares no conflict of interest.

Nomenclature

u, v, w	velocity components	r, φ, z	coordinate axes
σ	electrical conductivity	B_0	magnetic field strength
μ	dynamic viscosity	ρ_f	density of base fluid
β_T	thermal expansion coefficient	β_C	concentration expansion coefficient
ν	kinematic viscosity	g^*	acceleration due to gravity
L_1	velocity slip coefficient	L_2	temperature slip coefficient
L_3	concentration slip coefficient	Ω	constant angular velocity
T	temperature	C	concentration
T_w	wall temperature	C_w	wall concentration
T_∞	ambient fluid temperature	C_∞	ambient fluid concentration
α_m	thermal diffusivity	k	thermal conductivity
$(\rho c)_p$	effective heat capacity of nanoparticles	$(\rho c)_f$	heat capacity of fluid
D_B	Brownian diffusion coefficient	D_T	thermophoretic diffusion coefficient
E_a	activation energy	n	fitted rate constant

k_r	reaction rate	κ	Boltzmann constant
ζ	similarity variable	f', g	dimensionless velocities
θ	dimensionless temperature	ϕ	dimensionless concentration
Sc	Schmidt number	Ha	Hartman number
λ_T	thermal buoyancy number	Pr	Prandtl number
N_b	Brownian motion parameter	N_t	thermophoresis parameter
λ_C	concentration buoyancy number	α	velocity slip parameter
β	thermal slip parameter	γ	concentration slip parameter
E	dimensionless activation energy	δ	temperature difference parameter
C_f, C_g	skin friction coefficients	Re_r	local rotational Reynolds number
Nu	Nusselt number	Sh	Sherwood number

References

1. Choi, S.U.S. *Enhancing Thermal Conductivity of Fluids With Nanoparticles*; FED 231/MD; Argonne National Lab.: Lemont, IL, USA, 1995; Volume 66, pp. 99–105.
2. Buongiorno, J. Convective transport in nanofluids. *J. Heat Transf.* **2006**, *128*, 240–250.
3. Eastman, J.A.; Choi, S.U.S.; Li, S.; Yu, W.; Thompson, L.J. Anomalously increased effective thermal conductivities of ethylene glycol-based nanofluids containing copper nanoparticles. *Appl. Phys. Lett.* **2001**, *78*, 718–720.
4. Tiwari, R.K.; Das, M.K. Heat transfer augmentation in a two-sided lid-driven differentially heated square cavity utilizing nanofluid. *Int. J. Heat Mass Transf.* **2007**, *50*, 2002–2018.
5. Abu-Nada, E.; Oztop, H.F. Effects of inclination angle on natural convection in enclosures filled with Cu-water nanofluid. *Int. J. Heat Fluid Flow* **2009**, *30*, 669–678.
6. Mansur, S.; Ishak, A. Three-dimensional flow and heat transfer of a nanofluid past a permeable stretching sheet with a convective boundary condition. *AIP Conf. Proc.* **2014**, *1614*, 906–912.
7. Hayat, T.; Muhammad, T.; Alsaedi, A.; Alhuthali, M.S. Magnetohydrodynamic three-dimensional flow of viscoelastic nanofluid in the presence of nonlinear thermal radiation. *J. Magn. Magn. Mater.* **2015**, *385*, 222–229. [CrossRef]
8. Mahanthesh, B.; Gireesha, B.J.; Gorla, R.S.R. Nonlinear radiative heat transfer in MHD three-dimensional flow of water based nanofluid over a non-linearly stretching sheet with convective boundary condition. *J. Niger. Math. Soc.* **2016**, *35*, 178–198. [CrossRef]
9. Hayat, T.; Aziz, A.; Muhammad, T.; Alsaedi, A. On magnetohydrodynamic three-dimensional flow of nanofluid over a convectively heated nonlinear stretching surface. *Int. J. Heat Mass Transf.* **2016**, *100*, 566–572.
10. Muhammad, T.; Alsaedi, A.; Shehzad, S.A.; Hayat, T. A revised model for Darcy-Forchheimer flow of Maxwell nanofluid subject to convective boundary condition. *Chin. J. Phys.* **2017**, *55*, 963–976.
11. Hayat, T.; Muhammad, T.; Shehzad, S.A.; Alsaedi, A. On magnetohydrodynamic flow of nanofluid due to a rotating disk with slip effect: A numerical study. *Comp. Methods Appl. Mech. Eng.* **2017**, *315*, 467–477. [CrossRef]
12. Sheikholeslami, M.; Kataria, H.R.; Mittal, A.S. Radiation effects on heat transfer of three dimensional nanofluid flow considering thermal interfacial resistance and micro mixing in suspensions. *Chin. J. Phys.* **2017**, *55*, 2254–2272. [CrossRef]
13. Muhammad, T.; Alsaedi, A.; Hayat, T.; Shehzad, S.A. A revised model for Darcy-Forchheimer three-dimensional flow of nanofluid subject to convective boundary condition. *Results Phys.* **2017**, *7*, 2791–2797. [CrossRef]
14. Hayat, T.; Sajjad, R.; Muhammad, T.; Alsaedi, A.; Ellahi, R. On MHD nonlinear stretching flow of Powell-Eyring nanomaterial. *Results Phys.* **2017**, *7*, 535–543. [CrossRef]
15. Ellahi, R.; Zeeshan, A.; Hussain, F.; Abbas, T. Study of shiny film coating on multi-fluid flows of a rotating disk suspended with nano-sized silver and gold particles: A comparative analysis. *Coatings* **2018**, *8*, 422. [CrossRef]
16. Selimefendigil, F.; Oztop, H.F. Mixed convection of nanofluids in a three dimensional cavity with two adiabatic inner rotating cylinders. *Int. J. Heat Mass Transf.* **2018**, *117*, 331–343. [CrossRef]

17. Muhammad, T.; Lu, D.C.; Mahanthesh, B.; Eid, M.R.; Ramzan, M.; Dar, A. Significance of Darcy-Forchheimer porous medium in nanofluid through carbon nanotubes. *Commun. Theoret. Phys.* **2018**, *70*, 361. [CrossRef]
18. Suleman, M.; Ramzan, M.; Ahmad, S.; Lu, D.; Muhammad, T.; Chung, J.D. A numerical simulation of silver-water nanofluid flow with impacts of Newtonian heating and homogeneous-heterogeneous reactions past a nonlinear stretched cylinder. *Symmetry* **2019**, *11*, 295. [CrossRef]
19. Asma, M.; Othman, W.A.M.; Muhammad, T. Numerical study for Darcy-Forchheimer flow of nanofluid due to a rotating disk with binary chemical reaction and Arrhenius activation energy. *Mathematics* **2019**, *7*, 921. [CrossRef]
20. Asma, M.; Othman, W.A.M.; Muhammad, T.; Mallawi, F.; Wong, B.R. Numerical study for magnetohydrodynamic flow of nanofluid due to a rotating disk with binary chemical reaction and Arrhenius activation energy. *Symmetry* **2019**, *11*, 1282. [CrossRef]
21. Saif, R.S.; Hayat, T.; Ellahi, R.; Muhammad, T.; Alsaedi, A. Darcy-Forchheimer flow of nanofluid due to a curved stretching surface. *Int. J. Numer. Methods Heat Fluid Flow* **2019**, *29*, 2–20. [CrossRef]
22. Ellahi, R.; Zeeshan, A.; Hussain, F.; Abbas, T. Thermally charged MHD bi-phase flow coatings with non-Newtonian nanofluid and Hafnium particles along slippery walls. *Coatings* **2019**, *9*, 300. [CrossRef]
23. Moradikazerouni, A.; Hajizadeh, A.; Safaei, M.R.; Afrand, M.; Yarmand, H.; Zulkifli, N.W.B.M. Assessment of thermal conductivity enhancement of nano-antifreeze containing single-walled carbon nanotubes: Optimal artificial neural network and curve-fitting. *Phys. A* **2019**, *521*, 138–145. [CrossRef]
24. Asadi, A.; Aberoumand, S.; Moradikazerouni, A.; Pourfattah, F.; Żyła, G.; Estelle, P.; Mahian, O.; Wongwises, S.; Nguyen, H.M.; Arabkoohsar, A. Recent advances in preparation methods and thermophysical properties of oil-based nanofluids: A state-of-the-art review. *Powder Technol.* **2019**, *352*, 209–226. [CrossRef]
25. Alsarraf, J.; Moradikazerouni, A.; Shahsavar, A.; Afrand, M.; Salehipour, H.; Tran, M.D. Hydrothermal analysis of turbulent boehmite alumina nanofluid flow with different nanoparticle shapes in a minichannel heat exchanger using two-phase mixture model. *Phys. A* **2019**, *520*, 275–288. [CrossRef]
26. Vo, D.D.; Alsarraf, J.; Moradikazerouni, A.; Afrand, M.; Salehipour, H.; Qi, C. Numerical investigation of γ-AlOOH nano-fluid convection performance in a wavy channel considering various shapes of nanoadditives. *Powder Technol.* **2019**, *345*, 649–657. [CrossRef]
27. Ranjbarzadeh, R.; Moradikazerouni, A.; Bakhtiari, R.; Asadi, A.; Afrand, M. An experimental study on stability and thermal conductivity of water/silica nanofluid: Eco-friendly production of nanoparticles. *J. Clean. Prod.* **2019**, *206*, 1089–1100. [CrossRef]
28. Ma, Y.; Shahsavar, A.; Moradi, I.; Rostami, S.; Moradikazerouni, A.; Yarmand, H.; Zulkifli, N.W.B.M. Using finite volume method for simulating the natural convective heat transfer of nano-fluid flow inside an inclined enclosure with conductive walls in the presence of a constant temperature heat source. *Phys. A* **2019**, 123035. [CrossRef]
29. Von Karman, T. Uber laminare and turbulente Reibung. *ZAMM Z. Angew. Math. Mech.* **1921**, *1*, 233–252. [CrossRef]
30. Turkyilmazoglu, M.; Senel, P. Heat and mass transfer of the flow due to a rotating rough and porous disk. *Int. J. Thermal Sci.* **2013**, *63*, 146–158. [CrossRef]
31. Rashidi, M.M.; Kavyani, N.; Abelman, S. Investigation of entropy generation in MHD and slip flow over rotating porous disk with variable properties. *Int. J. Heat Mass Transf.* **2014**, *70*, 892–917. [CrossRef]
32. Turkyilmazoglu, M.; Nanofluid flow and heat transfer due to a rotating disk. *Comput. Fluids* **2014**, *94*, 139–146. [CrossRef]
33. Hatami, M.; Sheikholeslami, M.; Gangi, D.D. Laminar flow and heat transfer of nanofluids between contracting and rotating disks by least square method. *Powder Technol.* **2014**, *253*, 769–779. [CrossRef]
34. Mustafa, M.; Khan, J.A.; Hayat, T.; Alsaedi, A. On Bödewadt flow and heat transfer of nanofluids over a stretching stationary disk. *J. Mol. Liq.* **2015**, *211*, 119–125. [CrossRef]
35. Sheikholeslami, M.; Hatami, M.; Ganji, D.D. Numerical investigation of nanofluid spraying on an inclined rotating disk for cooling process. *J. Mol. Liq.* **2015**, *211*, 577–583. [CrossRef]
36. Doh, D.H.; Muthtamilselvan, M. Thermophoretic particle deposition on magnetohydrodynamic flow of micropolar fluid due to a rotating disk. *Int. J. Mech. Sci.* **2017**, *130*, 350–359. [CrossRef]
37. Aziz, A.; Alsaedi, A.; Muhammad, T.; Hayat, T. Numerical study for heat generation/absorption in flow of nanofluid by a rotating disk. *Results Phys.* **2018**, *8*, 785–792. [CrossRef]

38. Hayat, T.; Ahmad, S.; Khan, M.I.; Alsaedi, A. Modeling and analyzing flow of third grade nanofluid due to rotating stretchable disk with chemical reaction and heat source. *Phys. B* **2018**, *537*, 116–126. [CrossRef]
39. Qayyum, S.; Imtiaz, M.; Alsaedi, A.; Hayat, T. Analysis of radiation in a suspension of nanoparticles and gyrotactic microorganism for rotating disk of variable thickness. *Chin. J. Phys.* **2018**, *56*, 2404–2423. [CrossRef]
40. Hayat, T.; Khalid, H.; Waqas, M.; Alsaedi, A. Numerical simulation for radiative flow of nanoliquid by rotating disk with carbon nanotubes and partial slip, Comput. *Methods Appl. Mech. Eng.* **2018**, *341*, 397–408. [CrossRef]